Cascadia Tremor Located Near Plate Interface Constrained by S Minus P Wave Times

Mario La Rocca, *et al.*

Science **323**, 620 (2009);
DOI: 10.1126/science.1167112

particles are single-domain NCs. Also, the lattice parameter of 0.401 (± 0.001) nm obtained for the alloy NPs agrees very well with the value expected from Vegard's law, that is, a linear interpolation of the lattice parameters of Au and Pt [see the discussion of this point in (*22*)], if a solid solution had formed. After the Au leaching step, the lattice parameter decreased to 0.391 (± 0.001) nm, in agreement with the known lattice parameter of pure Pt [0.392 nm (*29*)]. Thus, full dealloying of the Au-Pt-nanoalloy could be achieved. We note that a partial dealloying by an electrochemical method has been recently reported by Koh and Strasser (*31*).

As a final point, we discuss the catalytic activity of the Pt NCs affixed to the surface of the SPBs. Previous work (*23*, *32*, *33*) showed that the catalytic reduction of *p*-nitrophenol to *p*-aminophenol can be used for the analysis of the catalytic activity of Pt NPs. We assumed that reduction rates were independent of the concentration of sodium borohydride because it was in excess compared to *p*-nitrophenol. Moreover, the apparent rate constant, k_{app}, was found to be proportional to the surface *S* of the Pt NPs present in the system (*32*, *33*):

$$-\frac{dc_t}{dt} = k_{app}c_t = k_1 S c_t \qquad (1)$$

where c_t is the concentration of *p*-nitrophenol at time *t* and k_1 is the rate constant normalized to *S*, the surface area normalized to the unit volume of the system. k_1 is plotted against the specific surface *S* of the Pt NCs in the systems in Fig. 4 (*32*). The Pt NCs exhibit a high catalytic activity and turnover numbers as high as 1580 ± 50, which are among the highest turnover numbers measured so far for this reaction (*23*, *32*, *33*). Hence, the composite particles consisting of the SPBs and the Pt NCs present a system with high colloidal stability that may be used for catalysis in an aqueous environment.

References and Notes

1. C. Burda, X. Chen, R. Narayanan, M. A. El-Sayed, *Chem. Rev.* **105**, 1025 (2005).
2. S. K. Ghosh, T. Pal, *Chem. Rev.* **107**, 4797 (2007).
3. R. Jin *et al.*, *Science* **294**, 1901 (2001).
4. Y. Sun, Y. Xia, *Science* **298**, 2176 (2002).
5. R. Narayanan, M. A. El-Sayed, *J. Am. Chem. Soc.* **126**, 7194 (2004).
6. N. Tian, Z.-Y. Zhou, S.-G. Sun, Y. Ding, Z. L. Wang, *Science* **316**, 732 (2007).
7. S. C. Warren *et al.*, *Science* **320**, 1748 (2008).
8. E. Sulman *et al.*, *Top. Catal.* **39**, 187 (2006).
9. T. S. Ahmadi, Z. L. Wang, T. C. Green, A. Henglein, M. A. El-Sayed, *Science* **272**, 1924 (1996).
10. R. Narayanan, M. A. El-Sayed, *J. Am. Chem. Soc.* **126**, 7194 (2004).
11. R. Narayanan, M. A. El-Sayed, *J. Phys. Chem. B* **107**, 12416 (2003).
12. R. Narayanan, M. A. El-Sayed, *Nano Lett.* **4**, 1343 (2004).
13. Y. Sun, L. Zhuang, J. Lu, X. Hong, P. Liu, *J. Am. Chem. Soc.* **129**, 15465 (2007).
14. I. Pastoriza-Santos, L. Liz-Marzan, *Nano Lett.* **2**, 903 (2002).
15. M. Turner *et al.*, *Nature* **454**, 981 (2008).
16. H. Lee *et al.*, *Angew. Chem. Int. Ed.* **45**, 7824 (2006).
17. S. Kinge, H. Bönnemann, *Appl. Organomet. Chem.* **20**, 784 (2006).
18. J. Ren, R. D. Tilley, *Small* **3**, 1508 (2007).
19. E. Ramirez, L. Eradés, K. Philippot, P. Lecante, B. Chaudret, *Adv. Funct. Mater.* **17**, 2219 (2007).
20. S. Guo, Y. Fang, S. Dong, E. Wang, *J. Phys. Chem. C* **111**, 17104 (2007).
21. J. Snyder, P. Asanithi, A. B. Dalton, J. Erlebacher, *Adv. Mater.* **20**, 4883 (2008).
22. M. Schrinner *et al.*, *Adv. Mater.* **20**, 1928 (2008).
23. M. Ballauff, *Prog. Polym. Sci.* **32**, 1135 (2007).
24. Y. Lu *et al.*, *J. Phys. Chem. C* **111**, 7676 (2007).
25. R. Ferrando, J. Jellinek, R. L. Johnston, *Chem. Rev.* **108**, 845 (2008).
26. M. Schrinner *et al.*, *Macromol. Chem. Phys.* **208**, 1542 (2007).
27. Z. Li, E. Kesselman, Y. Talmon, M. A. Hillmyer, T. P. Lodge, *Science* **306**, 98 (2004).
28. J. E. Huheey, *Inorganic Chemistry: Principles of Structure and Reactivity* (Pearson/Addison-Wesley, Boston, ed. 5, 2004).
29. D. Brooksbank, K. W. Andrews, *J. Iron Steel Inst. London* **206**, 595 (1968).
30. T. Swanson, *Natl. Bur. Stand. (U.S.) Circ.* **31**, 539 (1953).
31. S. Koh, P. Strasser, *J. Am. Chem. Soc.* **129**, 12624 (2007).
32. Y. Mei, Y. Lu, F. Polzer, M. Ballauff, F. Polzer, *Chem. Mater.* **19**, 1062 (2007).
33. Y. Mei *et al.*, *Langmuir* **21**, 12229 (2005).

34. Financial support by the Deutsche Forschungsgemeinschaft, SFB 481, Bayreuth; by the BASF SE; and by the Fonds der Chemischen Industrie is gratefully acknowledged. M.S. thanks the Minerva Foundation, the German Academic Exchange Service (DAAD), and the Technion Russell Berrie Nanotechnology Institute (RBNI) for the support during a stay at the Technion in Haifa. Y.T. thanks the von Humboldt Foundation for the support, through a von Humboldt–Meitner Prize, of the collaboration with the University of Bayreuth. Cryo-TEM was performed at the Hannah and George Krumholz Laboratory for Electron Microscopy of Soft Matter, part of the Technion Project on Complex Liquids, Microstructure, and Macromolecules. The HR-TEM work was done at the Electron Microscopy Center at the Department of Materials Engineering, the Technion.

Supporting Online Material

www.sciencemag.org/cgi/content/full/323/5914/617/DC1
Materials and Methods
Figs. S1 to S4
Table S1
References

2 October 2008; accepted 15 December 2008
10.1126/science.1166703

Cascadia Tremor Located Near Plate Interface Constrained by *S* Minus *P* Wave Times

Mario La Rocca,[1]* Kenneth C. Creager,[2] Danilo Galluzzo,[1] Steve Malone,[2] John E. Vidale,[2] Justin R. Sweet,[2] Aaron G. Wech[2]

Nonvolcanic tremor is difficult to locate because it does not produce impulsive phases identifiable across a seismic network. An alternative approach to identifying specific phases is to measure the lag between the *S* and *P* waves. We cross-correlate vertical and horizontal seismograms to reveal signals common to both, but with the horizontal delayed with respect to the vertical. This lagged correlation represents the time interval between vertical compressional waves and horizontal shear waves. Measurements of this interval, combined with location techniques, resolve the depth of tremor sources within ±2 kilometers. For recent Cascadia tremor, the sources locate near or on the subducting slab interface. Strong correlations and steady *S-P* time differences imply that tremor consists of radiation from repeating sources.

Deep nonvolcanic tremor (NVT) has been observed in several tectonically active regions. In Cascadia and Japan, a relation with the subduction dynamics is inferred by the contemporaneous occurrence of slow slip detected geodetically (*1*–*3*). In these regions, the occurrence of major episodic tremor and slip (ETS) events is surprisingly periodic (*2*). Minor NVT has been triggered by the stresses imposed by low-frequency seismic waves radiated by major distant earthquakes (*4*–*6*), and NVT is modulated by ocean tidal loading (*7*), indicating that small stress perturbations trigger it. NVT is characterized by low amplitudes, a lack of energy at high frequency, emergent onsets, an absence of clear impulsive phases, and durations from minutes to days. The lack of impulsive phases identifiable across seismic networks in Cascadia hinders accurate source location by conventional techniques.

NVT recorded in Shikoku, Japan, contains identifiable low-frequency earthquakes (LFEs) (*8*, *9*), suggesting that tremor is primarily made up of many back-to-back LFEs. On individual seismograms, *S* waves are sometimes identified. Stacking seismograms of repeating events recorded at a given station after aligning them on the *S* waves produces a clear *P* wave. The *S* minus *P* times allow an accurate depth to be determined. Such Japanese tremor locations are found to be near the subduction plate interface (*8*, *10*). Individual LFEs have not yet been reported in tremor recorded in Cascadia.

Tremor episodes that continue for several days are accompanied by geodetically observed slow slip in both Cascadia and Shikoku, leading

[1]Istituto Nazionale di Geofisica e Vulcanologia–Osservatorio Vesuviano, Via Diocleziano 328, 80124 Napoli, Italy. [2]Department of Earth and Space Science, University of Washington, Box 351310, Seattle, WA 98195, USA.

*To whom correspondence should be addressed. E-mail: mlarocca@ov.ingv.it

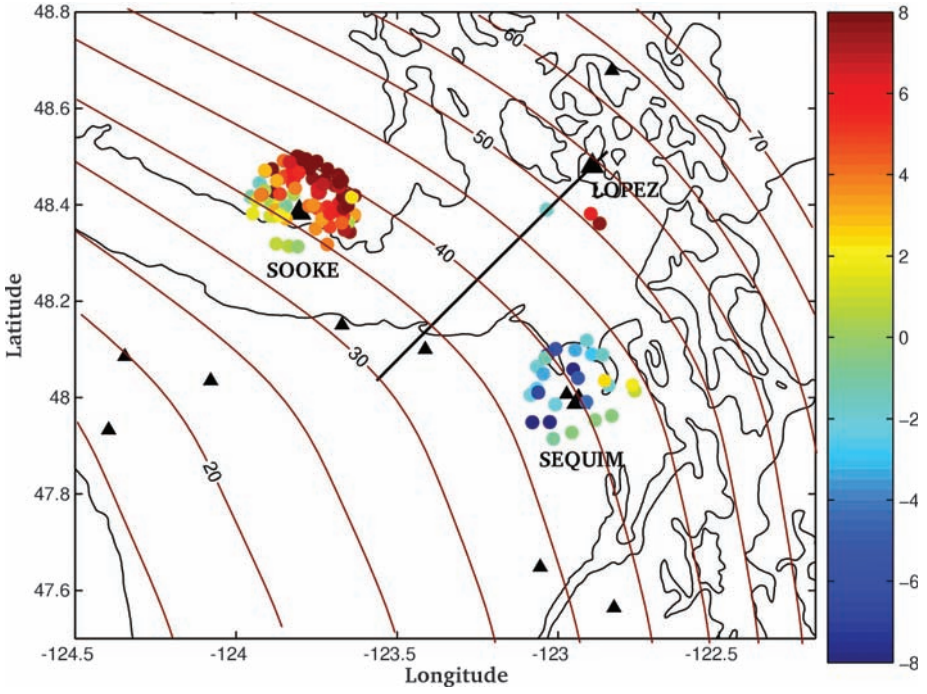

Fig. 1. Map showing locations of the three seismic arrays (large triangles), other stations used for location (small triangles), depth (km) to the plate interface [assumed to be 7 km above the slab Moho (*20*)], and location of cross section on Fig. 4 (black line) and tremor epicenters (dots), color-coded by distance above (red) and below (blue) the plate interface. Tremor epicenters are determined from cross-correlations of seismogram envelopes, and depths come from additional $t_{s\text{-}p}$ constraints. Theoretical ray incident angles at the arrays are restricted to be less than 15°.

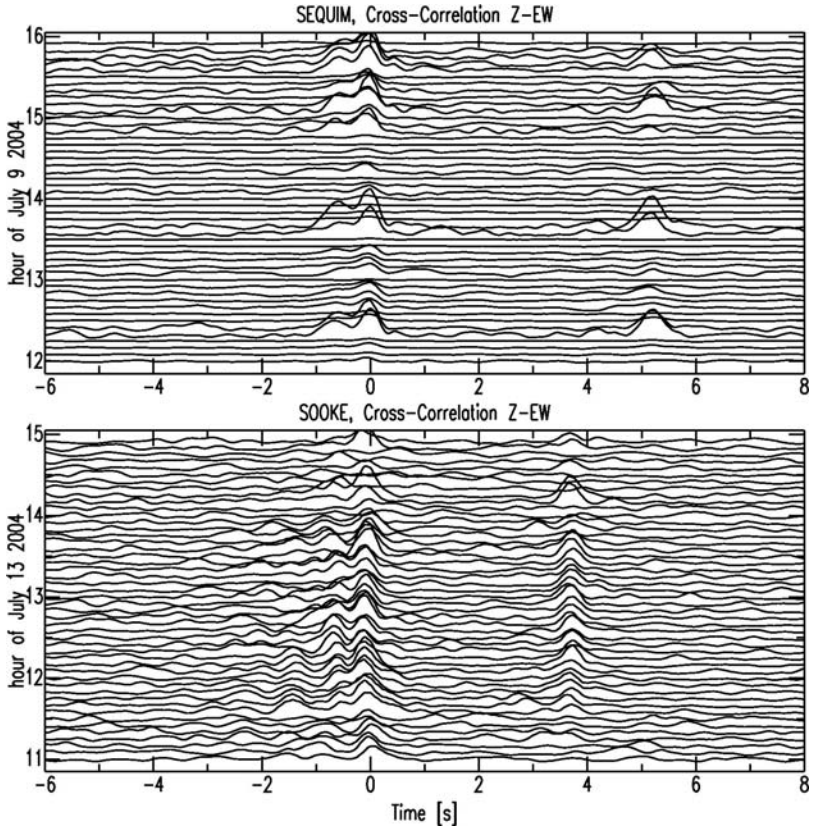

Fig. 2. Envelopes of the cross-correlations between vertical and east components for 5-min windows recorded at Sequim array (**top**) and Sooke array (**bottom**).

to the widely accepted interpretation for Japan that tremor and slow slip are manifestations of the same process. In contrast, attempts to locate tremor in Cascadia have resulted in a broad, 40-km-thick, distribution in depth, leading to the interpretation that much of the tremor is related to fluids throughout a large volume above the plate interface (*11*, *12*). Three different location techniques for tremor in Cascadia produce depth estimates over a range of 40 km. One technique uses the arrival times of seismic signal envelopes (*12*–*14*) and conventional location techniques based on an *S*-wave velocity model. A second technique, the Source Scanning Algorithm (*15*), stacks seismograms such that theoretical *S*-wave time delays correspond to a grid of possible source locations. Formal uncertainties are as small as 5 km but still show a wide depth range (*11*, *16*). A third technique uses small-aperture arrays to compute slowness vectors for seismic wavefronts and back projects those for a common source (*17*). In all of these cases, common signal shapes are processed under the assumption that they are direct *S* phases.

Cascadia tremor depth estimates likely have a greater uncertainty than the reported formal errors of 10 km in epicenter and more in depth. We tested this assumption by using two of the techniques to locate earthquakes in the same region as the tremor. The differences between the more accurately determined catalog earthquake depths and those we computed are much greater than the formal errors, sometimes tens of kilometers different (*14*, *17*). In the case of back projection of slowness vectors, unmodeled lateral velocity variations may bend the wave fronts sufficiently to explain these large errors in estimated tremor depths. Errors in depth determined from arrival times of seismogram envelopes are caused largely by unmodeled variations in *S*-wave coda duration. Here, we apply a new location procedure that greatly improves the depth resolution of the tremor sources.

Our data come from low-noise stations of the Pacific Northwest Seismograph Network and from three dense arrays composed of six three-component short-period seismic stations that were deployed specifically to record the July 2004 ETS event in Cascadia (*18*) (Fig. 1). Tremor periods with depths from 20 to 60 km have been reported (*12*, *16*, *17*). Polarization analysis of array data indicates that most of the signal has *S*-wave polarization (*13*) with apparent velocity higher than 5 km/s, as expected for shear waves from a deep source (*17*). *P*-wave polarization is observed in some of the tremor signals (*18*).

To improve the signal-to-noise ratio, we first stacked the seismograms over all the stations for each component of each array. Such stacks emphasize signals arriving with a steep incidence angle, i.e., from sources directly below an array. Then we computed the cross-correlations between the vertical and each horizontal stacked trace by using 300-s windows bandpass-filtered from

2 to 8 Hz. On many traces, the cross-correlogram envelopes show a distinct and persistent peak at positive lag times of 3.5 to 6.0 s, and no such peaks at negative lag times (Fig. 2). Positive lags correspond to the vertical component leading the horizontal component. These are particularly evident at the Sequim and Sooke arrays, where they were observed in many 5-min windows every day from 9 to 18 July. At the Lopez array, similar lags were visible only sporadically on 9 and 10 July, when tremor was nearest the array.

The distinct peaks at positive lags are consistent with the arrival of first vertical *P* waves and then horizontal *S* waves. The sequential correlations are characterized by tens of minutes with almost constant *S* minus *P* times ($t_{s\text{-}p}$). In several cases, when these peaks are most evident, visual inspection of the stacked seismograms revealed many subtle individual *P*- and *S*-wave arrival pairs with the same $t_{s\text{-}p}$ (Fig. 3). This pattern implies that at least some Cascadia tremor is made up of individual LFEs from a single source region occurring rapidly one after another in a sporadic sequence such as observed in Japan (*9*).

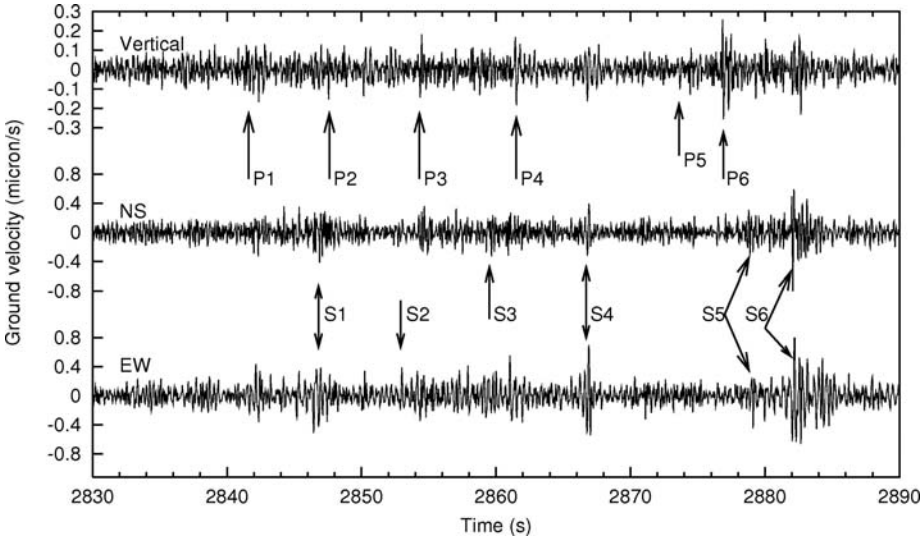

Fig. 3. Three-component seismograms in which several *P* waves, marked by arrows on the vertical component, are followed by *S* waves 5.1 ± 0.2 s later, as marked by arrows on the horizontal components. Seismograms are the stacked signals of Sequim array bandpass filtered between 2 and 10 Hz. The reference time is 15:00 GMT of 9 July 2004.

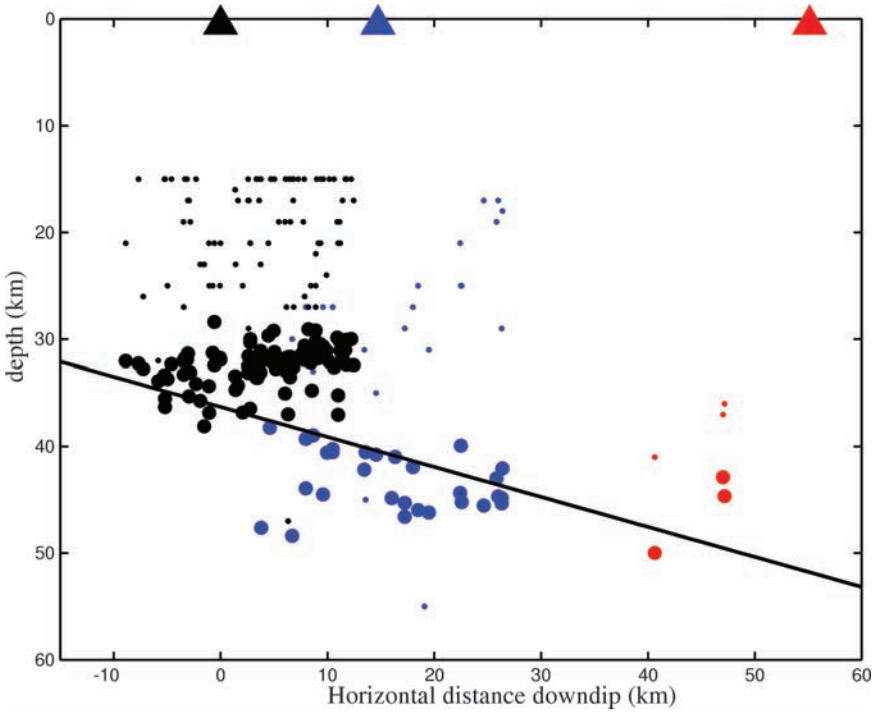

Fig. 4. Cross-section of tremors shown in Fig. 1 along the southwest-northeast profile. Small dots show hypocenters determined solely from envelope cross correlations. Large dots are hypocenters of the identical set of tremor periods, but with their depths shifted to satisfy the additional $t_{s\text{-}p}$ constraints from the Sooke (black), Sequim (blue), and Lopez (red) arrays.

Figure 2 shows lag times of 5.2 s at Sequim and of 3.7 s at Sooke. At Sequim, there were no intervals during the entire tremor period with $t_{s\text{-}p}$ less than 4.5 s. The low horizontal slowness measured at this array during times corresponding to $t_{s\text{-}p}$ near 4.5 s indicate that the sources were directly beneath the array. In contrast, higher slowness and back-azimuths to the north systematically correspond to $t_{s\text{-}p}$ = 5.0 to 5.4 s. At the Sooke array, all *S*-*P* times were between 3.7 and 4.4 s. The smallest value of $t_{s\text{-}p}$ = 3.7 s (Fig. 2) is consistent with sources located almost directly beneath the array. At the Lopez array, there were only a few periods of tremor with clear cross-correlation peaks, and those had $t_{s\text{-}p}$ = 5.5 s.

Combining the $t_{s\text{-}p}$-determined distances with slowness determined by array analysis allows an accurate estimate of the source depth. Based on a standard layered Earth model (*19*), tremor below the Sequim array ($t_{s\text{-}p}$ = 4.5 s) was located at a depth of 39 ± 2 km, whereas it was 31 ± 2 km below the Sooke array ($t_{s\text{-}p}$ = 3.7 s). To better compare the range of depths determined with and without the $t_{s\text{-}p}$ constraints, we applied an envelope cross-correlation tremor location method (*14*) to the same periods of time for which good *S*-*P* cross-correlation times are available. We located these tremor bursts both with and without the constraints of distance based on array measurements of $t_{s\text{-}p}$ and show the resulting epicenters in Fig. 1 and cross-section in Fig. 4. We kept all observations for which the theoretical ray angles at the arrays were less than 15° from the vertical. Depths are shown relative to the plate interface depth as determined from slab-Moho reflections (*20*). The depth range for locations determined with just envelope cross-correlations is large (small circles) as compared with those of the same tremor located with the additional $t_{s\text{-}p}$ constraints (large circles). At Lopez and Sequim, the refined depths are close to the plate interface. On average, the tremor beneath Sooke appears to be farther above the slab interface than that beneath Sequim and Lopez. This is likely an artifact of unmodeled high wave speeds associated with the Crescent Basalts beneath Sooke (*21*). Taken together, out of 128 observations, the mean source distance above the plate interface is 3 km and the standard deviation is ±5 km.

The clear correlations and stable $t_{s\text{-}p}$ in the signals suggest that, as was the case in Shikoku, where individual low-frequency events are found in the tremor and precisely located (*8*), at least some of the deep tremor in Cascadia consists of highly repetitive, continuous sequences of individual events, which radiate both *P*- and *S*-wave

energy from a volume small enough to give almost constant t_{s-p} over periods of tens of minutes or more. We cannot locate all tremor with this method for two reasons. First, the stable determination of t_{s-p} depends on tremor over an extended period coming from only one place, which is not always the case. Second, our technique is most sensitive to tremor beneath each array where the *P* and *S* waves are clearly separated into vertical and horizontal components. There are many periods of time, particularly at the Lopez array, in which tremor was located some distance from an array. In these cases, there was likely too much *S*-wave energy on the vertical component and *P* energy on the horizontal to get a strong cross-correlation. Although we cannot determine the depth of all observed tremor, the tremor under each array occurred near the subduction zone interface, and we see no evidence for shallow tremor, in contrast to other studies (*11*, *12*, *16*, *17*). Our method is ideally suited to find shallow tremor if it existed beneath an array.

If our results are representative of most NVT in Cascadia, then the contemporaneous occurrence of Global Positioning System–detected slow slip (*22*) indicates that deep tremor and slow slip are two manifestations of the same source process in Cascadia, as has been inferred for Japan (*8*, *10*, *23*). This hypothesis is further supported by the polarization characteristics of tremor signals, which are in good agreement with the expected polarization of signals produced by fault slip along the subduction megathrust (*13*).

References and Notes

1. K. Obara, *Science* **296**, 1679 (2002).
2. G. Rogers, H. Dragert, *Science* **300**, 1942 (2003).
3. K. Obara, H. Hirose, *Tectonophysics* **417**, 33 (2006).
4. J. L. Rubinstein *et al.*, *Nature* **448**, 579 (2007).
5. J. Gomberg *et al.*, *Science* **319**, 173 (2008).
6. M. Miyazawa, J. Mori, *Geophys. Res. Lett.* **32**, L10307 (2005).
7. J. L. Rubinstein, M. La Rocca, J. E. Vidale, K. C. Creager, A. G. Wech, *Science* **319**, 186 (2008).
8. D. R. Shelly, G. C. Beroza, S. Ide, S. Nakamula, *Nature* **442**, 188 (2006).
9. D. R. Shelly, G. C. Beroza, S. Ide, *Nature* **446**, 305 (2007).
10. Shelly D. R., G. C. Beroza, S. Ide, *Geochem. Geophys. Geosys.* **8** (2007).
11. H. Kao *et al.*, *Nature* **436**, 841 (2005).
12. W. McCausland, S. Malone, D. Johnson, *Geophys. Res. Lett.* **32**, L24311 (2005).
13. Wech A. G., K. C. Creager, *Geophys. Res. Lett.* **34**, L22306 (2007).
14. A. G. Wech, K. C. Creager, *Geophys. Res. Lett.* **35**, L20302 (2008).
15. H. Kao, S.-J. Shan, *Geophys. J. Int.* **157**, 589 (2004).
16. H. Kao *et al.*, *J. Geophys. Res.* **111**, B03309 (2006).
17. M. La Rocca *et al.*, *Bull. Seismol. Soc. Am.* **98**, 620 (2008).
18. M. La Rocca *et al.*, *Geophys. Res. Lett.* **32**, L21319 (2005).
19. R. S. Crosson, *J. Geophys. Res.* **81**, 3047 (1976).
20. L. A. Preston, K. C. Creager, R. S. Crosson, T. M. Brocher, A. M. Trehu, *Science* **302**, 1197 (2003).
21. K. Ramachandran, R. D. Hyndman, T. M. Brocher, *J. Geophys. Res.* **111**, B12301 (2006).
22. T. I. Melbourne, W. M. Szeliga, M. M. Miller, V. M. Santillan, *Geophys. Res. Lett.* **32**, L04301 (2005).
23. Ide S., D. R. Shelly, G. C. Beroza, *Geophys. Res. Lett.* **34**, L03308 (2007).

24. Istituto Nazionale di Geofisica e Vulcanologia and IRIS/PASSCAL provided instruments for the arrays; other seismograms were provided by the Pacific Northwest Seismic Network. Discussions with T. Pratt, J. Gomberg, H. Houston, A. Ghosh, E. Del Pezzo and comments from two anonymous reviewers improved this manuscript. Funding was provided by INGV, NSF and the U.S. Geological Survey.

13 October 2008; accepted 12 December 2008
10.1126/science.1167112

Divergent Evolution of Duplicate Genes Leads to Genetic Incompatibilities Within *A. thaliana*

David Bikard,[1] Dhaval Patel,[2] Claire Le Metté,[1] Veronica Giorgi,[1] Christine Camilleri,[1] Malcolm J. Bennett,[2] Olivier Loudet[1]*

Genetic incompatibilities resulting from interactions between two loci represent a potential source of postzygotic barriers and may be an important factor in evolution when they impair the outcome of interspecific crosses. We show that, in crosses between strains of the plant *Arabidopsis thaliana*, loci interact epistatically, controlling a recessive embryo lethality. This interaction is explained by divergent evolution occurring among paralogs of an essential duplicate gene, for which the functional copy is not located at the same locus in different accessions. These paralogs demonstrate genetic heterogeneity in their respective evolutionary trajectories, which results in widespread incompatibility among strains. Our data suggest that these passive mechanisms, gene duplication and extinction, could represent an important source of genetic incompatibilities across all taxa.

When crossing individuals from different species is feasible, offspring often have reduced viability or fertility (*1*, *2*). The Bateson-Dobzhansky-Muller model explains such incompatibilities on the basis of the synergistic interaction of genes that have functionally diverged among the respective parents (*3*–*5*). Elucidating the molecular basis of such genetic incompatibilities is of great importance to the science of evolution as well as to plant breeding. Whether these incompatibilities mostly appear concurrently with speciation (arising, for example, in geographically isolated populations) or after speciation has occurred as a consequence of their divergence remains a considerable question (*4*); it is now known that such incompatibilities can segregate within species first (*5*, *6*). A limited number of genes interacting to cause hybrid incompatibility have been identified at the molecular level, such as the *Lhr*/*Hmr* system responsible for lethality of male F1s from a cross between two *Drosophila* species (*7*). Recently, an interaction between *zeel-1* and *peel-1* loci was discovered to cause widespread genetic incompatibility among *Caenorhabditis elegans* strains (*8*). Also at the intraspecific scale, a typical dominant case of incompatibility in *Arabidopsis thaliana* has been identified that may establish a link between hybrid necrosis and the plant immune system (*9*).

While generating homozygous progeny from crosses between *A. thaliana* wild strains, it is frequently witnessed that physically unlinked loci do not always segregate independently and that, often, one homozygous allelic combination at two independent loci is rare or totally absent in the descendants of a specific cross (*10*, *11*). This phenomenon explains part of the segregation distortion inherited in such material and is viewed as the recessive version of Bateson-Dobzhansky-Muller–type incompatibilities, although other models than functional divergence could apply (*12*, *13*). Such epistasis-based recessive incompatibilities could result in reduced fitness in the progeny and limit the extent of rearrangements among parental genomes. Furthermore, if several incompatibilities were to segregate within a cross they should lead to conflicts between the genomes of diverged strains, which could result in isolating barriers and, ultimately, speciation (*14*, *15*).

A cross between the *Arabidopsis* reference accession Columbia-0 (Col) and the Cape Verde Island accession Cvi-0 (Cvi) was generated, and 367 F6 recombinant inbred lines (RILs) were genotyped, revealing that two pairs of unlinked loci did not segregate independently from each other (*10*). For both of these pairs, a specific combination of Col and Cvi alleles was not found in the RIL set, resulting in a transchromosomal linkage disequilibrium pattern (pseudo-LD) and exhibiting segregation distortion (fig. S1). By focusing on one of these two-locus interactions (labeled LD1 in fig. S1), we realized that a homozygous combination of the Col allele at the LD1.1

[1]Genetics and Plant Breeding, INRA, SGAP UR254, F-78026 Versailles, France. [2]Centre for Plant Integrative Biology, Division of Plant Sciences, School of Biosciences, University of Nottingham, Sutton Bonington Campus, Loughborough LE12 5RD, UK.

*To whom correspondence should be addressed. E-mail: loudet@versailles.inra.fr